High Harmonic Generation and Molecular Orbital Tomography in Multielectron Systems: Beyond the Single Active Electron Approximation

Serguei Patchkovskii,[1,*] Zengxiu Zhao,[2,†] Thomas Brabec,[2] and D. M. Villeneuve[1]
[1]National Research Council of Canada, 100 Sussex Drive, Ottawa, Ontario K1A 0R6, Canada
[2]Physics Department and Center for Research in Photonics, University of Ottawa, 150 Louis Pasteur, Ottawa, Ontario K1N 6N5, Canada
(Received 21 March 2006; published 22 September 2006)

It was recently shown that the highest molecular orbital of N_2 could be reconstructed from a series of high harmonic measurements. Existing theories of high harmonic generation and orbital tomographic imaging are based on the single active electron approximation that ignores essential quantum mechanical properties such as the indistinguishability of identical particles and the Pauli exclusion principle. We show that, when fully antisymmetrized multielectron wave functions and electronic relaxation in the cation are considered, molecular orbital tomography records the image of the Dyson orbital plus exchange contributions from inner shells. The mixing of contributions from more than one molecular orbital gives access to additional wave function information. By utilizing the exchange term, harmonic emission from a closed-shell 4-electron system can be interpreted as a complete Hartree-Fock wave function.

DOI: 10.1103/PhysRevLett.97.123003 PACS numbers: 33.80.Wz, 33.80.Rv

High harmonic generation (HHG) takes place during the interaction of intense femtosecond laser light with gas-phase atoms or molecules [1–3]. HHG from aligned molecules is sensitive to the angle of the molecular frame relative to the laser electric field polarization [4–8]. Recently, it was demonstrated [9] that this orientation dependence can be used to reconstruct the shape of the highest occupied molecular orbital (HOMO) from high harmonic spectra by means of a tomographic algorithm. The orbital interpretation of HHG experiments is a subject of some controversy [10].

The original orbital tomography work [9] used the single active electron (SAE) approximation, which ignores essential quantum mechanical properties such as the indistinguishability of electrons, the Pauli exclusion principle, and the antisymmetry of the total electronic wave function. We will show that molecular orbital tomography measures the Dyson orbital associated with the ionization channel. For small electronically rigid molecules, the Dyson orbital coincides with the HOMO. The indistinguishability of the electrons involved in the recombination process gives rise to additional terms in the transition dipole corresponding to electron exchange between the HOMO and inner bound orbitals. These transitions modify the observed image of the orbital. We reinterpret the N_2 tomography experiment and show that the $2\sigma_u$ orbital is imaged in addition to the $3\sigma_g$.

Furthermore, we show how the exchange terms can be used to retrieve additional wave function information in molecular orbital tomography experiments. A determination of the electronic structure of a 4-electron system such as LiH is possible through a single ionization channel.

High harmonic generation can be described using a simple semiclassical model involving three steps that occur within a half-optical cycle [11,12]: (i) tunnel ionization of the highest energy electron, (ii) acceleration of the free electron in the laser field, and (iii) recombination of the electron to the state from which it originated. The recombination step leads to emission of a photon. This is the so-called strong-field approximation (SFA) [12].

A number of approximations are inherent in the SFA, such as describing the continuum electron as a plane wave, neglect of correlations between the continuum and the ion core, and omission of memory effects and of molecular rotations. In this Letter, we revisit one of the approximations (SAE) and retain the phenomenological treatment for the remaining steps.

The SAE approximation assumes that only one electron is influenced by the laser field. All other electrons are assumed not to contribute to the interaction. This approximation is commonly applied to most strong-field phenomena. Harmonic generation in the SAE approximation is determined by the square of the recombination dipole matrix element between the bound state $\psi_0(\vec{r})$ and the continuum electron $\chi(\vec{r})$ [13]. The continuum wave function is taken as a plane wave expansion $\chi(\vec{r}) = \int a(\omega) e^{i\vec{k}\cdot\vec{r}} d\vec{k}$, where $a(\omega)$ is the complex amplitude of the recombining electron wave packet. Although plane waves form a complete basis set, a better approximation might be analytic solutions to the Coulomb-Volkov equation, which is an active area of research. Until such solutions become available, and because we have no *a priori* knowledge of the effective local potential, a plane wave expansion is used.

The emitted extreme ultraviolet (xuv) frequency is determined by the electron's wave number at the time of recombination, $\omega(k) = k^2/2$. In atomic units, the high harmonic emission rate is given by $W(\omega) \propto \omega^4 |a(\omega)\vec{d}_k|^2$, with $\vec{d}_k = \langle \psi_0 | \vec{r} | e^{i\vec{k}\cdot\vec{r}} \rangle$ being the transition dipole matrix element between the bound state and a plane wave.

The molecular orbital tomography experiment [9] is performed by first aligning the gas-phase molecule using

a laser pulse. The second, more intense, pulse ionizes the molecule and creates the high harmonic emission. By rotating the polarization of the aligning pulse, harmonic spectra are obtained for a set of angles of the molecular frame relative to the ionizing laser polarization axis. The amplitudes $a(\omega)$ are determined by recording the spectrum from a reference atom with the same ionization potential as the molecule under study and then dividing by the calculated transition dipole matrix elements for its highest occupied atomic orbital. After factoring $a(\omega)$ out of the measured harmonic spectra, a set of transition matrix elements $\vec{d}_k$ is obtained for a set of plane waves with wave vectors $\vec{k}$. The vector field $\vec{d}$ can be inverted in the molecular frame by an inverse Fourier transform to yield the vector

$$\vec{f} \equiv \int \vec{d}(\vec{k}) e^{-i\vec{k}\cdot\vec{r}} d\vec{k} = \psi_0(\vec{r})\vec{r}, \tag{1}$$

from which the 1-electron bound state wave function can be retrieved.

In the SAE model, the transition is between a single-electron ground state ψ_0 and a single-electron continuum state χ. In the multielectron model, we consider transitions between the n-electron ground state and the state consisting of the $(n-1)$-electron ion and the 1-electron continuum.

In most cases of experimental interest, the molecule being imaged is in a spatially nondegenerate singlet state, represented by the n-electron wave function Ψ_0. This wave function depends on the set of n space-spin coordinates $x_1 \ldots x_n$, where $x_i = (\vec{r}_i, \sigma_i)$. If the resulting cation is also spatially nondegenerate, and no competing ionization channels are present, the total time-dependent wave function of the system can be written as

$$\Psi(t) = C_0(t)\Psi_0 + C_+(t)\Psi_+, \tag{2}$$

$$\Psi_+ = \hat{\mathcal{A}} \frac{1}{\sqrt{2}} (\Psi_\alpha \chi_\beta - \Psi_\beta \chi_\alpha), \tag{3}$$

where $\chi_\sigma(x_n)$ is the 1-electron wave function of the recolliding electron, corresponding to the continuum wave function in the SAE model. The spatial part of χ_σ is the same for both values of the spin. It is combined with the spin functions $\alpha = \uparrow$ and $\beta = \downarrow$. The $(n-1)$-electron wave functions $\Psi_{\alpha,\beta}(x_1 \ldots x_{n-1})$ are the degenerate components of the Kramers doublet of the target ion. They are chosen as eigenfunctions of the $(n-1)$-electron $\hat{S}^2$ and $\hat{S}_z$ operators. The antisymmetrizer $\hat{\mathcal{A}}$ is given by $(1 - \sum_{j=1}^{n-1} \hat{P}_{jn})/\sqrt{n}$, where the operator $\hat{P}_{jn}$ interchanges electrons j and n. The origin of the coordinate system in Eqs. (2) and (3) should be taken at the barycenter of Ψ_0 [14].

The product ansatz for Ψ_+ [Eq. (3)] neglects dynamical correlation between the continuum electron and the ion core. This effect is negligible in electronically rigid molecules such as N_2 but may become significant in more polarizable systems. If necessary, the correlation can be incorporated in Eq. (2) by using a multichannel approach.

Using wave functions (2) and (3), the recombination matrix element $\vec{d}$ becomes

$$\vec{d} = \langle \Psi_0 | \sum_{i=1}^{n} \vec{r}_i | \Psi_+ \rangle + \text{c.c.}, \tag{4}$$

where the integration is over all electron coordinates.

By using the indistinguishability of the electrons and symmetry between the components of the Kramers doublet, Eq. (4) can be transformed to a sum of an effective 1-electron term $\vec{d}_1$ and an exchange correction term $\vec{d}_2$, given by

$$\vec{d} = \sqrt{2}(\vec{d}_1 + \vec{d}_2), \tag{5}$$

$$\vec{d}_1 = \langle \psi^D | \vec{r}_n | \chi_\beta \rangle, \tag{6}$$

$$\psi^D = \sqrt{n} \langle \Psi_\alpha | \Psi_0 \rangle, \tag{7}$$

$$\vec{d}_2 = -\sqrt{n} \sum_{j=1}^{n-1} \langle \Psi_0 | \vec{r}_n | \hat{P}_{jn} \Psi_\alpha \chi_\beta \rangle. \tag{8}$$

The effective 1-electron term $\vec{d}_1$ involves the ionization channel-specific Dyson orbital ψ^D. It is the only contribution retained for rapid photoionization processes [15–17]. This "strong orthogonality" assumption is justified by the asymptotically vanishing overlap of the wave functions of the ionized electron and the ion. The assumption does not apply to high harmonic generation, where the exchange term $\vec{d}_2$ gives significant contributions.

The general-case expressions for many-electron integrals (7) and (8) will be reported elsewhere [14]. Their qualitative interpretation becomes transparent if the relaxation of one-particle orbitals upon ionization can be neglected (Koopmans' approximation). Further, we assume that the wave functions Ψ_0 and Ψ_α can each be represented by a single Slater determinant spanned by the spin orbitals $\psi_1 \ldots \psi_{n-1}, \psi_n$ and $\psi_1 \ldots \psi_{n-1}$, respectively. In this notation, orbital ψ_n corresponds to the HOMO. Then

$$\psi^D \approx \psi_n, \tag{9}$$

$$\vec{d}_2 = \langle \vec{\varphi} | \chi_\beta \rangle, \tag{10}$$

$$\vec{\varphi} \approx -\sum_{l=1}^{n-1} \langle \psi_l | \vec{r} | \psi_n \rangle \psi_l + \sum_{l=1}^{n} \langle \psi_l | \vec{r} | \psi_l \rangle \psi_n, \tag{11}$$

where $\vec{\varphi} \equiv (\varphi_x, \varphi_y, \varphi_z)$ and the projection $\langle \vec{\varphi} | \chi_\beta \rangle \equiv (\langle \varphi_x | \chi_\beta \rangle, \langle \varphi_y | \chi_\beta \rangle, \langle \varphi_z | \chi_\beta \rangle)$. In Eq. (11), the first term arises from the transition dipole moment between occupied one-particle orbitals and the HOMO. The second contribution represents the permanent dipole moment of the molecule. In a centrosymmetric system, the second term vanishes for the natural choice of the origin.

Following the SAE derivation above, we take the inverse Fourier transform of $\vec{d}$ in Eq. (5). This yields the many-electron generalization of $\vec{f}$ in Eq. (1),

$$\vec{f} \equiv (f_x, f_y, f_z) = \psi^D \vec{r} + \vec{\varphi}. \quad (12)$$

For an electronically rigid diatomic molecule, high harmonic generation imaging is governed largely by the shape of the HOMO [see Eq. (9)] with corrections arising from the electron exchange between the continuum electron and the deeper lying electrons $\vec{\varphi}$. In more complex systems, electronic relaxation causes the orbitals describing the neutral and ionic ground states to become different, and the effective single-particle orbital being imaged is the Dyson orbital [Eq. (7)]. In this case, the exchange contributions are given by the inverse Fourier transform of Eq. (8), which presents a generalization of $\vec{f}$ in Eq. (12).

Because of the exchange term $\vec{\varphi}$, Eq. (12) must be solved for four quantities ψ^D, φ_x, φ_y, and φ_z and is underdetermined. Direct extraction of the HOMO is thus possible only if some or all of the exchange correction orbitals are negligible. At the same time, Eq. (12) shows that a HHG experiment contains information not only about the HOMO but also about the inner orbitals. This creates an opportunity to reconstruct additional orbitals from one set of measurements [Eq. (12)].

We will discuss possible approaches to measuring additional orbitals later. A significant part of the multielectron wave function can be recovered from HHG using just the HOMO ionization channel. We will illustrate this point in the following two examples. For the numerical calculation of the Dyson and exchange correction orbitals in Eq. (12), we use GAMESS [18]. All calculations use single-determinant, spin-restricted wave functions, cc-pVTZ [19] basis sets, and fully relaxed orbitals.

The first example is the lithium hydride molecule in the $^1\Sigma^+$ ground state. We will show that we can reconstruct the complete electronic structure of this molecule through HHG from the HOMO alone. The ground state determinant is spanned by the doubly occupied orbitals $\psi_{1\sigma}$ and $\psi_{2\sigma}$. The Dyson orbital for the first ionization channel is $\psi^D = 0.96\psi_{2\sigma}$. The factor 0.96 is due to orbital relaxation in the cation; see Eq. (7). The exchange correction along the molecular axis is $\varphi_z = -1.56\psi_{2\sigma} - 0.078\psi_{1\sigma}$. In LiH, the exchange correction vanishes for the perpendicular components f_x and f_y. Therefore, the pure Dyson orbital can be reconstructed from the equations for f_x or f_y. Once the $\psi_{2\sigma}$ orbital is determined by renormalizing the Dyson orbital, the $\psi_{1\sigma}$ orbital can be retrieved from the equation for f_z.

Note that this reconstruction procedure requires some *a priori* knowledge. Here we have used $\varphi_x = \varphi_y = 0$ and the fact that there is no $\psi_{1\sigma}$ contribution to the Dyson orbital. Nevertheless, it is remarkable that information on the lower lying $\psi_{1\sigma}$ orbital can be extracted without direct ionization from this orbital. As a result, the HHG data for the 2σ ionization channel in LiH can be used to recover an approximate wave function for this molecule, as long as it can be represented by a single determinant.

In closed-shell molecules with more than four electrons, observation of a single ionization channel is no longer sufficient to extract all one-particle orbitals of a single-determinantal wave function. Nevertheless, there exist molecules where more than one orbital can be reconstructed from the high harmonic measurement of the HOMO. Only orbitals with a nonzero dipole transition element with the HOMO can be reconstructed. For example, tomographic reconstruction of the experimental data $\vec{f}$ from the HOMO ionization channel in N_2 yields two scalar fields:

$$\zeta_1 = \frac{1}{2}\left\{\frac{f_x}{x} + \frac{f_z}{z}\right\} = \psi^D + \frac{1}{2}\left\{\frac{\varphi_x}{x} + \frac{\varphi_z}{z}\right\}, \quad (13)$$

$$\zeta_2 = f_z - \frac{z}{x} f_x = \varphi_z - \frac{z}{x}\varphi_x. \quad (14)$$

The calculated Dyson orbital in N_2 is dominated by the HOMO, $\psi^D = 0.98\psi_{3\sigma_g} - 0.03\psi_{2\sigma_g}$. The calculated Dyson orbital and the $3\sigma_g$ HOMO in Fig. 1(b) are indistinguishable to the eye. The longitudinal exchange correction is $\varphi_z = -1.50\psi_{2\sigma_u} - 0.08\psi_{1\sigma_u}$. The transverse corrections are much smaller, $\varphi_x(\varphi_y) = -0.32\psi_{1\pi_{u,x}}(\psi_{1\pi_{u,y}})$.

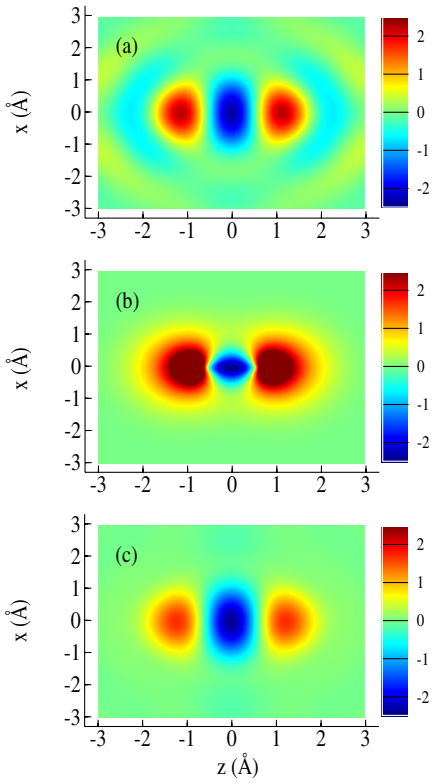

FIG. 1 (color online). One-particle orbitals integrated along the third (y) dimension are shown, using the same color scale on all panels. (a) The experimentally recovered wave function from Ref. [9]. (b) The $3\sigma_g$ orbital of N_2. (c) The predicted measurement [ζ_1, Eq. (13)] using the multielectron theory of high harmonic generation. Images (b) and (c) were processed with a band-pass Fourier filter, matching the experimentally observed range of harmonics.

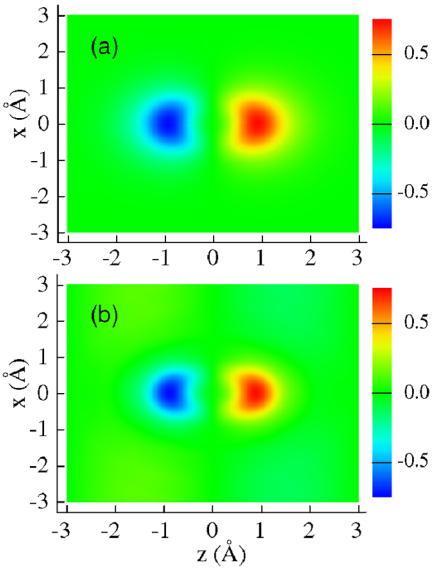

FIG. 2 (color online). (a) Simulated reconstruction of the quantity ζ_2 [Eq. (14)], based on the calculated $\vec{f}$ dipole field. The reconstructed orbital is scaled by a factor of 0.9. (b) Calculated $2\sigma_u$ molecular orbital in N_2. Both images are processed with a band-pass Fourier filter (see Fig. 1).

In the original work [9], the quantity ζ_1 was reconstructed. Our results show that ζ_1 is not the pure HOMO. The calculated ζ_1 is shown in the lower panel in Fig. 1 and is in better agreement with the experiment.

In N_2, exchange contributions are relatively small, and the retrieved quantity ζ_1 is qualitatively similar to the HOMO. The second experimentally observable quantity ζ_2 [Eq. (14)] vanishes identically in the SAE approximation. Because it is obtained as a difference of two quantities of similar magnitude, ζ_2 is more sensitive to noise than ζ_1. Unfortunately, experimental data collected in Ref. [9] are not sufficient for a reliable reconstruction. Instead, in Fig. 2, we give the result of tomographic reconstruction from the *calculated* $\vec{f}$ dipole field (top panel). The composition of the φ_x and φ_z exchange corrections indicates that ζ_2 is closely related to the nonbonding $2\sigma_u$ 1-particle orbital (bottom panel).

High harmonic generation from the N_2 HOMO allows us to probe only two orbital terms in the electronic structure. If additional ionization channels are induced in the system (such as channels leading to the low-lying $A^2\Pi_u$ and $B^2\Sigma_u^+$ excited states of the N_2^+ cation), it may be possible to reconstruct a single-determinantal approximate wave function of N_2 and other small molecules as well.

The multielectron theory that has been developed here shows that the recombination process central to high harmonic generation includes essential electron exchange effects that are not present in single active electron models. These contributions are due to electron indistinguishability and remain significant even when the inner electrons are strongly bound and are not excited by the driving laser field. Multielectron effects of the same origin should be expected in other recollision processes driven by strong laser fields, such as nonsequential ionization.

The authors acknowledge valuable discussions with Misha Ivanov and Olga Smirnova, as well as funding from NSERC SRO Grant No. 5796-299403/03 and NSERC DG Grant No. 327147-2006.

*Electronic address: serguei.patchkovskii@nrc.ca
†Electronic address: zzhao@uottawa.ca

[1] A. L'Huillier and P. Balcou, Phys. Rev. Lett. **70**, 774 (1993).
[2] C. Lyngå, M. B. Gaarde, C. Delfin, M. Bellini, T. W. Hänsch, A. L'Huillier, and C.-G. Wahlström, Phys. Rev. A **60**, 4823 (1999).
[3] A. L'Huillier, D. Descamps, A. Johansson, J. Norin, J. Mauritsson, and C.-G. Wahlström, Eur. Phys. J. D **26**, 91 (2003).
[4] M. Lein, N. Hay, R. Velotta, J. P. Marangos, and P. L. Knight, Phys. Rev. Lett. **88**, 183903 (2002).
[5] M. Lein, P. P. Corso, J. P. Marangos, and P. L. Knight, Phys. Rev. A **67**, 023819 (2003).
[6] R. de Nalda, E. Heesel, M. Lein, N. Hay, R. Velotta, E. Springate, M. Castillejo, and J. P. Marangos, Phys. Rev. A **69**, 031804 (2004).
[7] J. Itatani, D. Zeidler, J. Levesque, M. Spanner, D. M. Villeneuve, and P. B. Corkum, Phys. Rev. Lett. **94**, 123902 (2005).
[8] T. Kanai, S. Minemoto, and H. Sakai, Nature (London) **435**, 470 (2005).
[9] J. Itatani, J. Levesque, D. Zeidler, H. Niikura, H. Pépin, J. C. Kieffer, P. B. Corkum, and D. M. Villeneuve, Nature (London) **432**, 867 (2004).
[10] W. H. E. Schwarz, Angew. Chem., Int. Ed. **45**, 1508 (2006).
[11] P. B. Corkum, Phys. Rev. Lett. **71**, 1994 (1993).
[12] M. Lewenstein, P. Balcou, M. Y. Ivanov, A. L'Huillier, and P. B. Corkum, Phys. Rev. A **49**, 2117 (1994).
[13] H. A. Bethe and E. E. Salpeter, *Quantum Mechanics of One- and Two-Electron Atoms* (Springer, Berlin, 1957).
[14] S. Patchkovskii, Z. Zhao, T. Brabec, and D. M. Villeneuve (to be published).
[15] B. T. Pickup, Chem. Phys. **19**, 193 (1977).
[16] Y. Öhrn and G. Born, Adv. Quantum Chem. **13**, 1 (1981).
[17] J. V. Ortiz, *Computational Chemistry: Reviews of Current Trends* (World Scientific, Singapore, 1997), Vol. 2, Chap. 1, pp. 1–61.
[18] M. W. Schmidt *et al.*, J. Comput. Chem. **14**, 1347 (1993).
[19] T. H. Dunning, Jr., Chem. Phys. **90**, 1007 (1989).